UNSYS digital

International Journal of Robotics and Mechatronics

Robust Hierarchical Control Strategy for Heaving Wave Energy Converters

Omsalama M. M. Saeed, Addy Wahyudie, and Mohammed A. Jama

Department of Electrical Engineering, United Arab Emirates University, UAE

***Abstract*—**Numerous reference-based control strategies have been developed for enhancing the captured and converted energy of the heaving wave energy converters (WECs). This study developed a hierarchical control strategy (HCS) that provided an optimal reference signal considering the different sea-states and constraints on the heaving buoy's elevation. The developed HCS is composed of a higher hierarchical controller (HHC) and a lower hierarchical controller (LHC). An optimal reference signal, for different combinations of wave specific heights and frequencies under elevation's constraints, is provided by the HHC. The buoy's output velocity is regulated by the LHC, based on the reference signal provided by the HHC. Robustness and tracking performance are achieved by the LHC. The present paper utilized a proportional-integral-derivative (PID) controller augmented with sliding mode control (SMC), known for its robustness capabilities, for implementing the LHC. The developed control strategy was validated using regular (monochromatic) and irregular (polychromatic) sea-states. Validation process also considered both nominal and perturbed and disturbed systems. The HCS showed effectiveness in enhancing the power train of the heaving WECs while respecting the physical limitations of the system.

***Keywords*—**Heaving wave energy converters, Hierarchical control strategy, Reference-based controller, Robust control, Sliding mode control.

I. Introduction

Ocean waves, as a resource of renewable energy, are of considerable potential. The total amount of power contained in them is estimated to be 2 terawatts (TW), reaching the same magnitude as the world's electricity consumption. According to conservative estimates, approximately 10-25 % of this total power can be harnessed, suggesting that wave power could represent a considerable addition to total energy resources [1].

Wave energy converters (WECs) capture the energy contained in ocean waves and use it to generate electricity. Numerous wave energy conversion concepts have been developed all over the world; the number of patented wave energy conversion techniques in Europe, Japan, and North America exceeds 1,000. Although the concepts and designs of WECs vary significantly, they can be classified into the following main types.

Corresponding author: Addy Wahyudie (e-mail: addy.w@uaeu.ac.ae).
This paper was submitted on December 3, 2015; revised on December 20, 2015; and accepted on December 27, 2015.

- Attenuator
- Point absorber
- Terminator

Point absorbers, considered in this paper, are floating structured devices that heave up and down. The mechanical energy contained in the wave is converted to electrical energy by the mean of power take-off mechanisms. There are different types of PTO systems, including rotary generators that employ energy transfer methods such as turbine transfer and hydraulic conversion. Direct electrical linear generators are also used [2]. This paper adopts the latter mechanism, along with the heaving point absorber, for the simplicity of the structure and the direct power conversion.

In order to improve the performance of WECs in terms of captured power, variety of control strategies have been deployed and proposed. Design requirements such as robustness, respecting system's limitations and supporting the PTO mechanism must be fulfilled by the proposed strategies [3]. Existing control strategies can be classified to open loop control (i.e., no feedback or reference signal to track) and reference-based control techniques. Passive control strategies such as resistive and reactive loading are open loop control techniques [4]. They are simple and cost effective. However, since these strategies are designed based on a single operating point (i.e., single frequency of the sea wave), the performance of the controlled system is degraded at other frequencies that exist in reality. Besides, other controllers such as fuzzy-based controllers and predictive control strategies have been proposed [5] [6] [7] [8]. In terms of providing optimum control effort and imposing system's constraints, predictive control strategies are very good candidates. Though, the high computations' cost of these strategies is a major disadvantage. In the second category, reference-based, a closed loop feedback is designed to track a reference signal. Based on the resonance theory, maximum power is achieved when the velocity of the buoy is in phase with the excitation force. Thus, calculated velocity of the excitation force has been selected as a reference signal in designing these types of controllers [9]. These techniques generally have an HCS structure which comprises two levels. A Higher Hierarchical Controller (HHC) which provides a reference signal. This signal is robustly tracked by a Lower Hierarchical Controller (LHC). A simple HCS was proposed in [10] where a lead compensator was used as a LHC, while

uncertainties were compensated for by using an ultra-local model principle. Other strategies employed internal mode control in the LHC to improve robustness [11] [12]. In [13], reference-based method and predictive control were combined. This was achieved by using Model Predictive Control (MPC) to generate the reference signal by the HHC.

In this paper, we propose a new technique to generate a reference signal by the HHC with a certain degree of adaptability to different sea-states. The reference velocity in [11] [12] [13] was generated based on the radiation resistance value of the buoy for a specific single wave's frequency. In reality, sea waves are irregular with different peak frequencies and significant heights. Thus, the latter approach has a major drawback in terms of adaptability. Lately, an approach of using the intrinsic resistance to generate the reference velocity has provided a solution to overcome the mentioned drawback [10] [14]. The value of the intrinsic resistance varies with the variations of the wave's peak frequency and specific height. However, it involves complex and high cost computations. In this study, a constrained optimization quadratic programming (QP) problem was formulated and solved off line to generate different values for the intrinsic resistance based on different sea-states. The objective of the problem was to maximize the absorbed energy subject to maximum elevation of the buoy. As a result, a look-up table was constructed and used in the HHC. This approach simplified and lowered the computational cost significantly and at the same time achieved adaptability while respecting the system's physical limitations. For the LHC, Sliding Mode Control (SMC) was utilized. This technique guarantees high robustness feature which compensates for model uncertainties and un-modelled parameters.

This paper is organized as follows: The mathematical model of the heaving WEC is illustrated in Section II. The proposed control strategy is explained in Section III. Other control strategies are considered for the sake of comparison Section IV. Simulation setup, results and analysis are discussed in Section V. Finally, the conclusion is in Section VI.

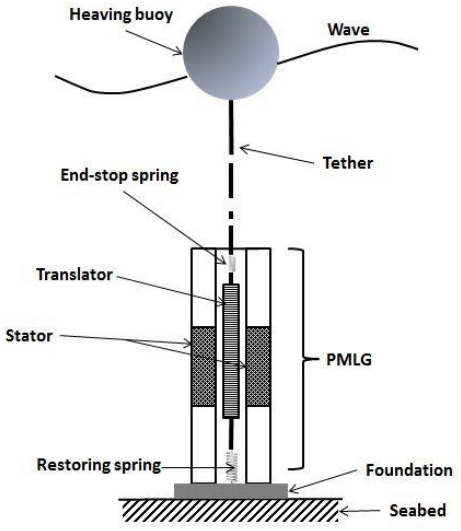

Figure 1 Heaving WEC structure

II. Mathematical Model

The overall system is modeled by two mathematical models: mechanical model and electrical model. The latter is out of the scope of this study. This work utilized the mechanical model of the system, which involves the control force, to develop the hierarchical control strategy of focus.

Structure of the adopted spherical buoy of Uppsala University [15] is shown on **Figure 2**. It is composed of a spherical floating body (buoy) connected through a tether to the translator of a permanent magnet linear generator (PMLG) that represents the power take-off (PTO) mechanism.

A. Mechanical Forces

The buoy is affected by numerous mechanical forces. Hydrodynamic forces due to the interaction between the buoy and the sea wave. And forces applied by the PTO. They can be summarized as follows:

- Hydrodynamic forces
  - Excitation force, $f_{ex}(t)$
  - Radiation force, $f_r(t)$
  - Hydrostatic buoyancy force, fb(t)
  - Drag force, $f_d(t)$
- Forces applied by the PTO
  - Control force, $f_u(t)$
  - Restoring force, $f_{rs}(t)$
  - Friction force, $f_f\ (t)$
  - End-stop force, $f_{es}(t)$

1) Excitation Force: The excitation force can be modeled, in terms of the undisturbed wave elevation ($\eta(t)$), in time domain by a bilateral convolution integral as follows

$$f_{ex}(t) = \int_{-\infty}^{\infty} k_{ex}(\tau - t)\eta(\tau)d\tau \qquad (1)$$

Applying Fourier transform on Equation 1, $f_{ex}(t)$ can be expressed in frequency-domain as

$$F_{ex}(j\omega) = K_{ex}(j\omega)H(j\omega)\ , \qquad (2)$$

where $K_{ex}(j\omega)$ is the frequency-domain wave excitation coefficient known as the excitation frequency response function (FRF), and $H(j\omega)$ is the Fourier transform of the wave elevation $\eta(t)$ [16]. Performing numerical solution using specialized software, WAMIT®, A linearized causal approximation for $K_{ex}(j\omega)$ is found as a transfer function of the form:

$$\widehat{K}_{ex}(j\omega) \approx \frac{N(s)}{D(s)} = \frac{b_m s^m + b_{m-1}s^{m-1} + \cdots + b_0}{s^n + a_{n-1}s^{n-1} + \cdots + a_0} \qquad (3)$$

where $\widehat{K}_{ex}(j\omega) \approx K_{ex}(j\omega)$. This results in an approximated excitation force, $\hat{F}_{ex}(j\omega)$, which is assumed to be equal to the actual one, $F_{ex}(j\omega)$.

2) Radiation Force: Cummins [17] proposed an expression for the time domain radiation force $f_r(t)$ for a vessel with zero forward speed as

$$f_r(t) = -m_\infty a(t) - \int_0^t K_r(t-\tau)v(\tau)d\tau \quad (4)$$

Several works have been conducted on how to handle the radiation convolution term in time-domain [16], [18]. In this study, the radiation convolution term is approximated by a fourth order linear state space model as follows

$$\dot{\boldsymbol{q}} = \mathbf{A}_r\boldsymbol{q}(t) + \mathbf{B}_r v(t) \quad (5)$$

$$\int_0^t k_r(t-\tau)v(\tau)d\tau \approx \mathbf{C}_r\boldsymbol{q}(t) \quad (6)$$

where $\boldsymbol{q}(t) \in \mathbb{R}^{4\times1}$ is the radiation state vector, the buoy's velocity $v(t) \in \mathbb{R}^{1\times1}$ is the input and the radiation force $\boldsymbol{f}_r(t) \in \mathbb{R}^{4\times1}$ is the model output. The state matrices of the model are $\mathbf{A}_r$, the radiation state matrix, $\mathbf{B}_r$,the radiation input matrix and $\mathbf{C}_r$, the radiation output matrix.

3) Hydrostatic buoyancy force: For a freely oscillating body, fb(t) is proportional to the body displacement from the equilibrium point and opposing the direction of the movement, that is

$$f_b(t) = -S_b z(t)\,, \quad (7)$$

where S_b is the buoyancy stiffness coefficient and is equal to $(\rho g A_w)$, and $A_w \approx \pi r^2$ where r is the radius of the spherical buoy.

4) Restoring force: Restoring force, $f_{rs}(t)$, is another spring force besides the previously mentioned hydrodynamic buoyancy spring force. It is acting on the sea-based PTO heaving WEC and results from the spring units placed between the linear moving translator and the sea-bed [19]. This force is directly proportional to the buoy displacement, $z(t)$ as follows

$$f_{rs}(t) = -S_{rs} z(t)\,, \quad (8)$$

where S_{rs} is the restoring spring coefficient.

5) Non-linear forces: Drag force $f_d(t)$, friction force $f_f\ (t)$ and end-stop force $f_{es}(t)$ are all non-linear forces [20], [21], [22], [23]. The system is approximated by a linear state-space model, as explained in subsection II-B, and assumed to be operated in linear mode. Hence, the effect of all non-linear forces will not be included in the model.

B. State Space Model

A state space model for the heaving spherical WEC is developed based on the hydrodynamic and mechanical forces that govern the buoy's motion and its interaction with sea waves. In a state space model, a system can be modeled using a set of nonlinear differential equations of the following general form

$$\dot{\boldsymbol{x}} = \boldsymbol{f}(t, \boldsymbol{x}, \boldsymbol{u})\,, \quad (9)$$

where $\boldsymbol{f} \in \mathbb{R}^{n\times1}$ is an n^{th} order vector of nonlinear functions, $\boldsymbol{x} \in \mathbb{R}^{n\times1}$ is the n^{th} order state vector, and $\boldsymbol{u} \in \mathbb{R}^{n\times1}$ is the m^{th} order input vector [24].

For our heaving WEC system, the system states are the buoy's heave (vertical) position and its velocity, $z(t)$ and $v(t)$ respectively. The first one can be measured by the mean of sensors, while the latter can be computed online using the position measurements. These are the main state variables that will be involved in the design. There are more four fictitious states though. The other four, as discussed earlier, resulted from the method used to model the radiation force, $f_r(t)$, and impose it to the state model. Thus the system's proposed model is of six state space variables and hence it is a sixth order system. As position and velocity represent the main state variables, all the forces that dictate the interaction between the buoy and the surrounding water were expressed as a function of these two variables in previous section, except for the wave excitation force, $f_{ex}(t)$, which is independent on the buoy dynamics. Using Newton's second law, all forces acting on the buoy and the PMLG translator can be formulated as

$$f_{ex}(t) - f_r(t) - f_b(t) - f_{rs}(t) + f_u(t) = ma(t) \quad (10)$$

Accordingly, the state space model can be formulated as follows:

$$\mathbf{A} = \begin{bmatrix} 0 & 1 & \mathbf{0}_{1\times4} \\ \dfrac{-(S_b+S_{rs})}{m+m_\infty} & \dfrac{-\alpha_v}{m+m_\infty} & \dfrac{-\mathbf{C}_r}{m+m_\infty} \\ \mathbf{0}_{4\times1} & \mathbf{B}_r & \mathbf{A}_r \end{bmatrix} \in \mathbb{R}^{6\times6}$$

$$\mathbf{B} = \begin{bmatrix} 0 \\ \dfrac{1}{m+m_\infty} \\ \mathbf{0}_{4\times1} \end{bmatrix} \in \mathbb{R}^{6\times1}$$

$$\mathbf{C} = [0 \quad 1 \quad \mathbf{0}_{1\times4}] \in \mathbb{R}^{1\times6}$$

where α_v represents the losses resistance that counts for any un-modeled losses, m is the mass of the buoy and $m_\infty$is the infinite added mass.

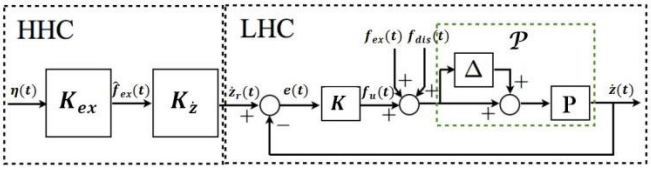

Figure 2 System's configuration

Maximum power absorption of a heaving WEC is achieved if the velocity of the buoy $v(t) = \dot{z}(t)$ is in phase with the excitation force $f_{ex}(t)$. This is known as the resonance condition resulting from the impedance matching principle, based on which, we can formulate the reference velocity as [25]

$$\dot{z}_r(t) = \frac{|f_{ex}(t)|}{2R_{int}(\omega)} cos\theta\,, \quad (11)$$

where θ is the phase difference between $f_{ex}(t)$ and $\dot{z}_r(t)$, and it equals zero at resonance. Usually, the constant $R_{int}(\omega)$ in

Equation 11 is selected from the maximum value of R_{int} over a range of operating frequencies.

III. Hierarchical Control Strategy (HCS)

In order to obtain resonance status, the control force generated by the PMLG, $f_u(t)$, is used. This results in a well-known drawbacks of the approach in Equation 11. The constant R_{int} is selected from one frequency only. Thus, high level of $f_u(t)$ due insufficient damping of $f_{ex}(t)$ can be caused. In the reactive control strategies, the high level control is undesirable because it enlarges the size of the PTO and reduces the efficiency of WEC systems. In the worst case condition, a high level of $f_u(t)$ can cause power reverse. Which means, we can reach a point where the PTO acts as a motor rather than a generator. In order to avoid these drawbacks, hierarchical control strategy (HCS) is proposed.

A. Higher Hierarchical Controller via Quadratic Programming (QP)

Instead of using Equation 11, which has its drawbacks for constant R_{int} as discussed, a constrained optimization problem is formulated, where the objective function is to maximize the absorbed energy E_{abs} subject to constrains on the buoy's maximum displacement z_m [26]. This is accomplished by formulating a constrained quadratic programming problem (QP) and solving it across a finite window n_w as follows

$$\max E_{abs} = T_s \sum_{i=0}^{n_w-1} [P_{ex}(k+i|k) - P_r(k+i|k)] \qquad (12)$$

where T_s is the sampling time, $P_{ex}(k+i|k)$ and $P_r(k+i|k)$ are the predicted excitation power and radiation power at time $(k+i)$, respectively. This relation can be expressed in terms of the buoy velocity,

$$E_{abs} = T_s \sum_{i=0}^{n_w-1} \left[\tilde{f}_{ex}(k+i|k) - f_r(k+i|k)\right]\dot{z}_r(k+i|k)\,, \qquad (13)$$

$f_r(k+i|k)$ is assumed to be equal to the radiation kernel of Equation 5. Thus, by replacing $f_r(k+i|k)$ with

$$f_r(k+i|k) = \mathbf{C}\boldsymbol{x}(k+i|k)\,, \qquad (14)$$

where $\boldsymbol{x}(k+i|k)$ is the state vector of the overall system at time $(k+i)$ and $\mathbf{C} = [\mathbf{0}_{1\times 2} \quad \mathbf{C}_r]$ Sequentially forward solving $f_r(k+i|k)$ across n_w-sized optimization window, we get

$$\mathbf{F}_r = \boldsymbol{\Theta}_1\boldsymbol{x}(k) + \boldsymbol{\Theta}_2\mathbf{V}\,, \qquad (15)$$

where

$$\mathbf{F}_r = \begin{bmatrix} f_r(k|k) \\ \vdots \\ f_r(k+n_w-1|k) \end{bmatrix}, \mathbf{V} = \begin{bmatrix} \dot{z}_r(k|k) \\ \vdots \\ \dot{z}_r(k+n_w-1|k) \end{bmatrix},$$

$$\boldsymbol{\Theta}_1 = [\mathbf{C} \quad \mathbf{CA} \quad \cdots \quad \mathbf{CA}^{n_w-1}]^T \in \mathbb{R}^{n_w\times 6}\,,$$

$$\boldsymbol{\Theta}_2 = \begin{bmatrix} 0 & 0 & \cdots & \cdots & 0 \\ \mathbf{CB} & 0 & \cdots & \cdots & 0 \\ \mathbf{CAB} & \mathbf{CB} & \ddots & \ddots & \vdots \\ \vdots & \ddots & \ddots & \ddots & \vdots \\ \mathbf{CA}^{n_w-1}\mathbf{B} & \cdots & \mathbf{CAB} & \mathbf{CB} & 0 \end{bmatrix} \in \mathbb{R}^{n_w\times n_w}\,,$$

$$\mathbf{A} = \begin{bmatrix} \mathbf{0}_{2\times 2} & \mathbf{0}_{2\times 4} \\ \mathbf{0}_{4\times 2} & \mathbf{A}_r \end{bmatrix}, \mathbf{B} = \begin{bmatrix} 1 \\ 0 \\ \mathbf{B}_r \end{bmatrix}.$$

A constrained QP problem with a decision variable, V, can be obtained by rewriting Equation 13 into the vector form and combining it with Equation 15 as

$$\begin{aligned} &minimize\ E_{abs} = \mathbf{V}^T\boldsymbol{\Theta}_2\mathbf{V} + \left(\boldsymbol{\Theta}_1 x(k) - \hat{\mathbf{F}}_{ex}\right)^T V\,, \\ &subject\ to\ \boldsymbol{\Xi}\mathbf{V} \le \boldsymbol{\Omega}\,, \end{aligned} \qquad (16)$$

where

$$\hat{\mathbf{F}}_{ex} = \begin{bmatrix} \hat{f}_{ex}(k|k) \\ \vdots \\ \hat{f}_{ex}(k+n_w-1|k) \end{bmatrix}, \qquad \boldsymbol{\Xi} = [-\mathbf{M} \quad \mathbf{M}]^T\,,$$

$$\boldsymbol{\Omega} = [z_m + \mathbf{P}\boldsymbol{x}(k) \quad z_m - \mathbf{P}\boldsymbol{x}(k)]^T\,.$$

The estimated excitation force across n_w is contained in $\hat{\mathbf{F}}_{ex}$. All the values in the latter are set to be fixed and equal to $\hat{f}_{ex}(k|k)$ as no prediction algorithm is used. The matrices used in the constraint inequality $\mathbf{M}$ and $\mathbf{P}$ are similar to $\boldsymbol{\Theta}_2$ and $\boldsymbol{\Theta}_1$, respectively, Except for the minor modification: $\mathbf{C} = [1 \quad \mathbf{0}_{1\times 5}]$. Equation 16 is minimized with respect to the future velocity trajectory $\mathbf{V}$, while limiting the buoy excursion to $\pm z_m$. The formulated QP is convex due to the fact that the Hessian matrix in Equation 16 is positive-definite [27].

It is very complicated and challenging task to solve Equation 16 in real-time. Instead, solving it off-line for various expected wave peak frequency ω_p and wave significant height H_s values, is simpler, cheaper and less computationally intensive solution. Then, the resultant sub-optimal continuous velocity profile is used to compute the sub-optimal intrinsic resistance, R_{qp}^*, as follows

$$\frac{1}{R_{qp}^*} = \left.\frac{\Re\{|\dot{z}_r|e^{j\omega t}\}}{\Re\{|f_{ex}|e^{j\omega t}\}}\right|_{\omega=\omega_p}\,, \qquad (17)$$

where $|f_{ex}|$ and $|\dot{z}_r|$ are the complex amplitudes of $f_{ex}(t)$ and $\dot{z}_r(t)$, respectively. The reciprocal of R_{qp}^* is used to avoid $R_{qp}^* \Rightarrow \infty$ at $\dot{z}_r(t) = 0$. A look-up table is constructed to adjust R_{qp}^* in real-time. The time-averaged sub-optimal resistance $\bar{R}_{qp}^*$ is calculated for monochromatic sea-states of different ω_p and H_s.

B. Lower Hierarchical Controller via PID augmented with SMC

This method considers using a stabilizing proportional-integral-derivative (PID) controller with association of Sliding Mode Controller (SMC) to achieve stability and robustness.

1) PID Controller: Conventional methods for synthesizing PID controller, such as root locus or adhoc, can be used. The form of the controller is

$$K(s) = k_p + \frac{k_i}{s} + k_d s \tag{18}$$

where k_p , k_i and k_d are the proportional, integral and derivative gains respectively.

2) Sliding Mode Controller: In the lower control loop SMC is deployed due to its remarkable tracking and robustness capability [24]. The proposed SMC is derived using the following procedure. Let us define the sliding surface $s(t)$ as

$$s(t) = \left(\frac{d}{dt} + \lambda\right)^{n-1} e(t) = 0\,,$$

where $e(t)$ is the error, n is the order of the system, and λ is a positive constant for ensuring the convergence to the sliding surface. In our case, the WEC system is second order system. Therefore, the sliding surface is formulated as

$$s(t) = \dot{e}(t) + \lambda e(t) = 0\,. \tag{19}$$

Due to mismatches between nominal model and the actual system, the term k1sgn(s(t)) is added to this control signal for handling model imperfections. The new control signal is

$$f_u(t) = k_d\dot{e}(t) + k_p e(t) + k_i \int e(t)dt + k_1 sgn(s(t)) \tag{20}$$

where $sgn(s(t))$ is the signum function of $s(t)$:

$$sgn\big(s(t)\big) = \begin{cases} sgn\big(s(t)\big) = +1 & if\ s(t) > 0 \\ sgn\big(s(t)\big) = -1 & if\ s(t) < 0 \end{cases}$$

The constant k_1 is a positive real number. A larger value of k_1 allows larger set of perturbation. However, a large value of k_1 will magnify the control force. Therefore, the value of k_1 is carefully selected by considering the trade-off between perturbations and the allowable level of $f_u(t)$.

In the practical point of view, this chattering is undesirable because the actuator cannot respond to sudden changes in the commanded control force. Also, the high frequency components in the chattering might evoke undesirable mechanical vibrations in the system. In order to avoid this, the addition term can be smoothed using the approximation method in [24]. By defining a thin boundary layer surface as

$$B(t) = \{\mathbf{w}, |s(\mathbf{w}; t)| \le \Phi\} \quad \Phi > 0\,,$$

where $\mathbf{w} = [z(t) \quad \dot{z}(t)]^T$, $B(t)$ is a layer that contains the chattered control force, Φ is the boundary layer thickness, and $\epsilon = \Phi/\lambda^{n-1}$ is the boundary layer width as depicted in **Figure 3**. The chattered control input in $B(t)$ is interpolated by replacing the term $sgn(s(t))$ by saturation function $sat(s(t))$. The saturation function is defined as follows:

$$sat\big(s(t)\big) = \begin{cases} sgn\big(s(t)\big) & if\ |s(t)| > \Phi \\ s(t)/\Phi & if\ |s(t)| < \Phi \end{cases}$$

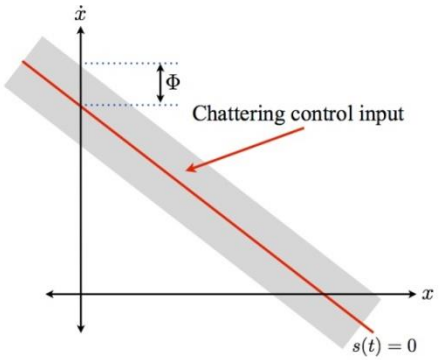

Figure 3 Chattering control force in the sliding surface

Therefore, the robust SMC with continuous control input for the WECs is formulated as

$$f_u(t) = k_d\dot{e}(t) + k_p e(t) + k_i \int e(t)dt + k_1 sat(s(t)) \tag{21}$$

In order to obtain the parameters kd, kp and ki of the PID controller, we can use conventional methods for designing the parameters of the PID controllers. Otherwise, we can use a systematic mathematical method that provides sets of stabilizing parameters. This method is known as real polynomial stabilization.

IV. Other Control Strategies

Two existing control strategies were selected for the sake of comparison in the results and analysis in Section V.

A. Resistive Loading (RL)

This is a very simple control strategy for the heaving WEC. It is based on producing a control force that is linearly proportional to the buoy velocity [28]. The optimum power transfer occurs when the PTO reactance cancels that of the intrinsic system reactance, leaving out the resistance terms. A simplified sub-optimal approach is to model the PTO impedance as a pure frequency dependent resistance, $R_c(\omega)$. Therefore, the control force can be represented as

$$f_u(t) = -R_c(\omega)v(t). \tag{22}$$

The easiest approach to determine $R_c(\omega)$ is by computing the magnitude of the system intrinsic impedance, $|Z_{int}(\omega)|$, thus we obtain [29]

$$f_u(t) = -|Z_{int}(\omega)|v(t). \tag{23}$$

where

$$|Z_{int}(\omega)| = \sqrt{(R_{int}(\omega))^2 + (X_{int}(\omega))^2}$$

B. Conventional Hierarchical Control System

Considering the following formula for calculating the reference velocity:

$$v_r(t) = \dot{z}_r(t) = \frac{\hat{f}_{ex}(t)}{2R_r} cos\theta\,, \tag{24}$$

where Rr and θ are the system's resistance and the phase difference between $\hat{f}_{ex}(t)$ and $\dot{z}_r(t)$, respectively.

The conventional hierarchical control system (C-HCS) is an HCS that utilizes Equation 24 in its higher level controller to generate the reference. The value of Rr is fixed for the whole range of operating frequencies and wave's significant heights.

V. Results and Discussion

This section shows the simulation's setup, results and analysis of the HCS in consideration, using QP method as an HHC to provide the reference signal, and PID augmented with SMC as an LHC to achieve tracking performance and robustness as explained in section III. Throughout this section, the convention QP-SMC will be used for this control strategy. Simulation's results show the complete system's performance under nominal conditions in various sea-states, and test it under system's perturbations and external disturbance. Besides, a comparison with existing controller techniques is presented. Simulation is carried out using MATLAB® Simulink®.

A. Simulation Setup and Verification Techniques

The system configuration of **Figure 2** is considered. The heaving spherical wave energy converter of Uppsala University [15] is considered with the detailed parameters' values shown in **Table I**.

The excitation force transfer function, $F_{ex}(s)$ of **Figure 2** is obtained as

$$\frac{F_{ex}(s)}{H(s)} = \frac{-2145s^7 + 1.2\times10^4 s^6 + \cdots}{s^8 + 0.9s^7 + 2.8s^6 + 1.5s^5 + 2.3s^4 + \cdots} \frac{-4.9\times10^4 s^5 + 3.9\times10^4 s^4 + \cdots}{0.7s^3 + 0.7s^2 + \cdots} \frac{4.2\times10^4 s^3 + 1.3\times10^4 s^2 - 5979s}{0.1s + 0.06} \quad (25)$$

where $F_{ex}(s)$ and $H(s)$ are the Laplace transform of $f_{ex}(t)$ and $\eta(t)$, respectively.

The state space model of Subsection II-B is used with $\alpha_v = R_{loss}$, where R_{loss} is the losses resistance. The mechanical model can be obtained with the following components of the radiation force:

$$\mathbf{A}_r = \begin{bmatrix} -3.4376 & -6.3533 & -4.9714 & -1.7168 \\ 1 & 0 & 0 & 0 \\ 0 & 1 & 0 & 0 \\ 0 & 0 & 1 & 0 \end{bmatrix}$$

$$\mathbf{B}_r = [1 \quad 0 \quad 0 \quad 0]^T$$

$$\mathbf{C}_r = [0.96\times10^5 \quad 3.62\times10^5 \quad 1.57\times10^5 \quad 0]$$

Solving the optimization problem of subsection III-A using quadratic programming, different values for intrinsic resistance based on different sea-states was found as shown in **Table II** and the corresponding **Figure 9**.

Table I Mechanical and Electrical Parameters of the WEC

Parameter (symbol)	Value unit
Buoy's Radius (r)	5 m
Buoy and translator mass (m_b)	2.68×10^5 kg
Infinite added mass (m_∞)	1.34×10^5 kg
Water plane area (A_w)	78.54 m^2
Submerged Volume (V_s)	261.8 m^3
Sea water density (ρ)	1025 kg/m^3
Gravitational acceleration (g)	9.81 m/s^2
Seabed depth (d)	80 m
Resonance angular frequency (ω_p)	1.56 rad/s
Buoyancy stiffness coefficient (S_b)	7.89×10^5 N/m
Nominal restoring stiffness coefficient (S_{rs0})	2×10^5 N/m
Nominal losses resistance (R_{loss0})	0.4×10^5 $N.s/m$
PMLG synchronous resistance (R_s)	0.29 Ohm
Permanent magnet flux (λ_{PM})	23 Wb
PMLG pole width (p_w)	0.05 m
DC link voltage (V_{dc})	3500 V
Modulation index (ma)	1

Table II The Lookup Table for the Value of R^*_{qp} in MNs/m based on Quadratic Programming (QP) Method

ω_p rad/s	$H_s = 1$ m	$H_s = 2$ m	$H_s = 3$ m
0.50	0.1900	0.3660	0.4360
0.55	0.1680	0.3300	0.4000
0.60	0.1560	0.3000	0.3910
0.65	0.1400	0.2800	0.3740
0.70	0.1300	0.2600	0.3540
0.75	0.1190	0.2500	0.3400
0.80	0.1040	0.2400	0.3300
0.85	0.0999	0.2200	0.3100
0.90	0.0960	0.2100	0.2920
0.95	0.0900	0.2000	0.2800
1.00	0.0830	0.1900	0.2730

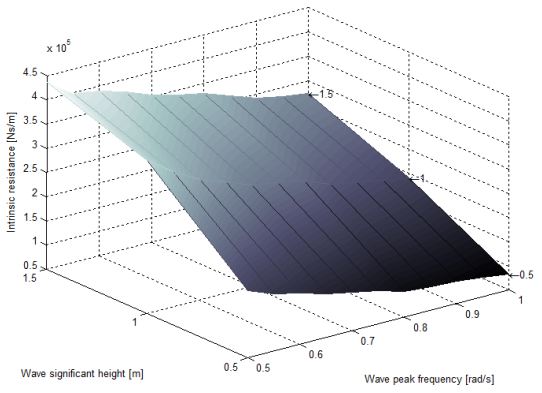

Figure 4 Intrinsic resistance

Parameters of the PID augmented with SMC are obtained and the resultant $f_u(t)$ is

$$f_u(t) = 100\dot{e}(t) + 1100e(t) + 1\times10^6\int e(t)dt + 1\times10^9 sat(s(t)) \quad (26)$$

The carried out simulation strategy can be summarized as:

1) Performance of nominal system in regular (monochromatic) sea-state of specific wave heights, Hs, of $1\,m$ and $3\,m$ for a range of peak frequencies (i.e., $0.5-1\,rad/s$). Plots of the values listed below vs. the specified peak frequency range were obtained, for both specific heights.
   - the average captured power, $\bar{P}_m$
   - the average electrical power, $\bar{P}_e$
   - the maximum control force, f_{um}
   - the maximum electrical power, P_{em}
   - the ration of maximum electrical power to the average electrical power, $P_{em}/\bar{P}_e$
   - the percentage of conversion efficiency between $\bar{P}_m$ and $\bar{P}_e$
2) Time domain response of nominal system in irregular (poly-chromatic) sea-state of peak frequency, $\omega_p = 0.7\,rad/s$, and specific wave height, $H_s = 2\ m$. Plots of this part includes the following measures in time interval $(20-140\ s)$:
   - reference and out velocities, $\dot{z}_r$ and $\dot{z}$ of the excitation force and the heaving buoy respectively
   - excitation force position, z, and output position of the heaving buoy, η
   - the control force and the excitation force, f_u and f_{ex} respectively
   - the mechanical captured power, P_m and its average, $\bar{P}_m$
   - the $d-q$ components of the stator voltage, v_{sq} and v_{sd}
   - the q-axis current component which implements the control force
   - the EMF voltage of the linear generator
   - the electrical converted power, P_e and its average, $\bar{P}_e$ where the first four items corresponds to the mechanical quantities and the last four corresponds to the electrical quantities.
3) Performance of the perturbed system under presence of disturbance force in irregular (poly-chromatic) sea-state of peak frequency, $\omega_p = 0.7\,rad/s$, and wave height,$H_s = 2\,m$. Result of this test is shown in a table that contains nine cases of perturbations and a tenth case, the worst case, where external disturbance force, $f_{dis}(t)$, is added. Performance in each case is measured in terms of energy drop percentage based on the energy calculated for the nominal case. Mean square error (MSE) is also calculated. In nominal case, value of the nominal restoring stiffness coefficient, R_{rs0}, is shown in **TABLE I**. The loss resistance, R_{loss}, is set to zero. For cases 1 through 9, the values of the restoring stiffness coefficient and the loss resistance are respectively set to

$$R_{rs} = R_{rs0} + \Delta_s \quad (27)$$

and

$$R_{loss} = R_{loss0} + \Delta_l \quad (28)$$

Then, the values $\Delta_s$and $\Delta_l$are varied from 0 % up to 50 %.In the worst case, the perturbation values are kept as in Case 9. Moreover, an external disturbance force, $f_{dis}(t)$, is added as a third input to the mechanical model (in addition to the excitation force, $f_{ex}(t)$, and the control force, $f_u(t)$) (see **Figure 2**). A disturbance force of magnitude of one third of the magnitude of the excitation force and same sea-state is generated using Simulink® as shown in **Figure 9**. This un-modelled disturbance force is formulated as

$$f_{dis} = -R_{loss}\dot{z}(t) - R_{rs0}z(t) - \alpha_d\dot{z}^2(t)\sin(\omega_d t) \quad (29)$$

where $\alpha_d = 0.5\times10^4$ and $\omega_d = 0.5\,rad/s$.

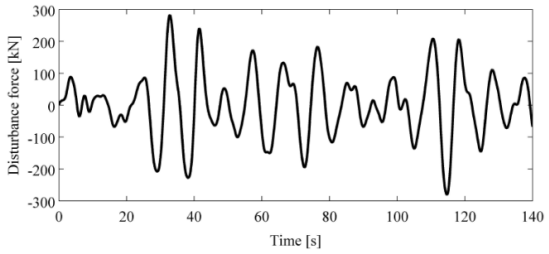

Figure 5 Disturbance force in irregular sea-state

B. Simulation Results and Discussion

System performance in nominal condition for wave significant heights, H_s, of $1\,m$ and $3\,m$ is shown in graphs of **Figure 7** and **Figure 8** respectively. Performance of the resistive loading method (RL) and the conventional HCS method, combined with SMC in the LHC, are added to the graphs for comparison. The convention CHCS-SMC is used for the latter.

For a significant height of $1\,m$, captured and converted average powers for both QP-SMC and CHCS-SMC are almost similar. They show results in the range of $50-170\,kW$ and $30-80\,kW$ respectively. While both values are very low, in comparison, in the case of RL (around $10\,kW$). The QP-SMC method maintained the physical constraints of the maximum allowable control force and the maximum value for the ratio $P_{em}/\bar{P}_e$, except for a very small region at low peak frequencies. However, the CHCS-SMC violated both constraints for more than the half region of the peak frequencies (i.e., up to almost $\omega_p = 0.8\,rad/s$). RL shows the best efficiency of above 60 %. The QP-SMC comes in the second place in terms of efficiency. But since the average captured and converted powers are much

larger in the case of QP-SMC than in the case of RL, the QP-SMC is more considerable though it has slightly less efficiency.

In the case of $H_s = 3\,m$, RL follows almost the same trend except for slight increase in the captured and converted powers. Performance of the CHCS-SMC is very bad as it works in reactive mode for the whole region. Which means it works as a motor rather than a generator, and hence consuming power all the time. The QP-SMC captures mechanical power in the range of $300 - 500\,kW$ and generating average electrical power in the range of $200 - 300\,kW$. It also shows efficiency in the same order of that of the RL (around 60 %). However, the constraint of the maximum control force is violated for peak frequency up to $0.7\,rad/s$.

The simulation results using the irregular sea-state using for mechanical and electrical quantities are shown in **Figure 8** and **Figure 9** respectively. The tracking capability of the SMC is demonstrated in **Figure 8(a)**. The figure shows that the velocity of the buoy $\dot{z}$perfectly matches the reference velocity,$\dot{z}_r$. The value of mean square error (MSE) is 2.19×10^{-5}. This indicates perfect tracking capability of the SMC. Considering the radius of the buoy, the elevation of the buoy z, and the wave elevation η in **Figure 8(b)**, we can see that the buoy's elevation reaches critical values, $1.5\,m$ at some points of the graph. **Figure 8(c)** shows a comparison between the control force $f_u(t)$ and the excitation force $f_{ex}(t)$. The control force has little bit higher order magnitude than the excitation force, $f_{ex}(t)$. It stays below its designed limitation for the specific sea-state used in this test. The instantaneous captured power $P_m$is shown in the **Figure 8(d)**. From the results, an average captured power $\bar{P}_m$ of $0.13\,MW$ is generated. The $d-q$ components of the stator voltage are shown in **Figure 9(a)**. The q-axis current component i_{sq} that implement the $f_u(t)$ is shown in **Figure 9(b)**. While **Figure 9(c)** shows the EMF voltage of the PTO. An average converted power $\bar{P}_e$ of $0.08\,MW$ is resulted by the PTO. It is shown in **Figure 9(d)**. This corresponds to 61.8 % of conversion efficiency from P_m to P_e.

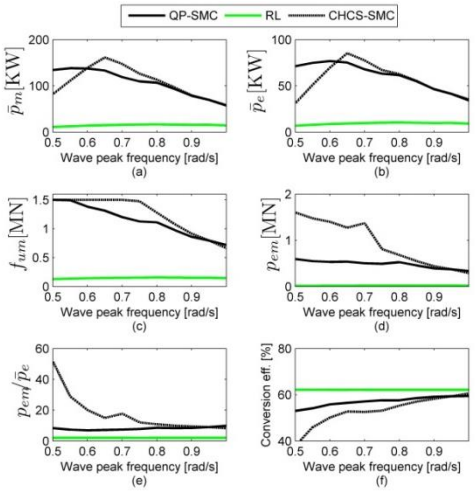

Figure 6 Simulation results of QP-SMC, RL and CHCS-SMC using monochromatic sea-state of $H_s = 1\,m$

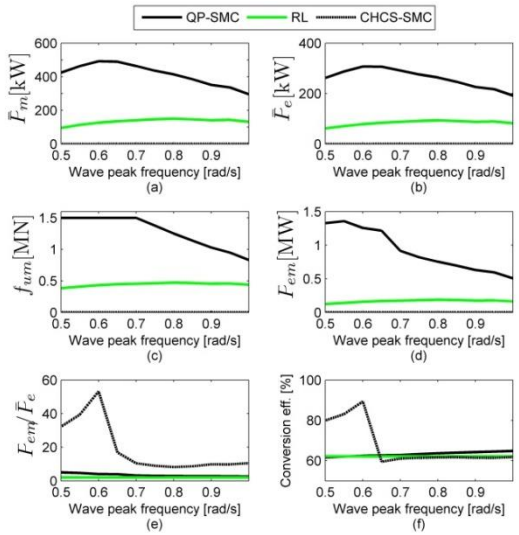

Figure 7 Simulation results of QP-SMC, RL and CHCS-SMC using monochromatic sea-state of $H_s = 3\,m$

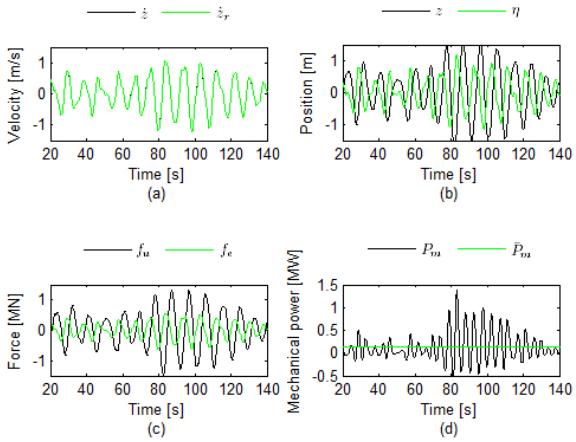

Figure 8 The simulation results of mechanical quantities using the QP-SMC under poly-chromatic sea-state with $H_s = 2\,m$ and $\omega_p = 0.7\,rad/s$

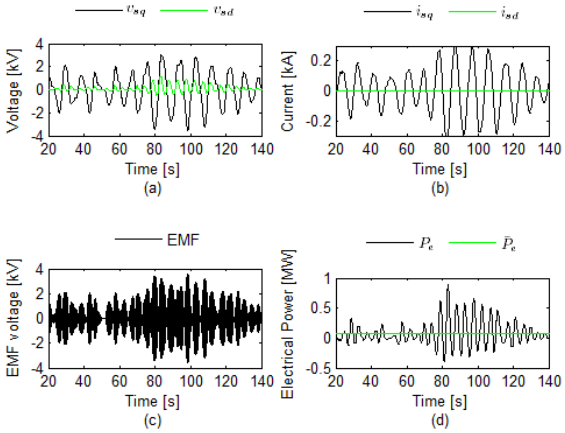

Figure 9 The simulation results of electrical quantities using the QP-SMC under poly-chromatic sea-state with $H_s = 2\,m$ and $\omega_p = 0.7\,rad/s$

Perturbation scenarios discussed in Subsection V-A are applied in the WEC system to test the tracking capability and robustness. Results are summarized in **TABLE III** in terms of energy drop percentage and MSE. Similar trend to that of the QP-LLC is noticed for the QP-AMC. The table shows that the energy drop increases slightly with increase in the restoring stiffness coefficient, R_s, while it increases significantly with the losses resistance, R_{sloss}. Tracking performance is good for some extend, but the MSE increases significantly for the case of 50 % perturbation in the restoring stiffness coefficient, R_s case 9.

TABLE III PERFORMANCE UNDER VARIOUS PERTURBATION SCENARIOS AND DISTURBANCE FORCE, WORST CASE, FOR THE QP-SMC

Cases	Δ_l (%)	Δ_s (%)	Energy (kW)	Energy Drop (%)	MSE ($x10^{-5}$)
Case 1	0	0	4.27	8.63	2.18
Case 2	0	0.25	4.27	8.67	2.28
Case 3	0	0.50	4.27	8.76	1.33
Case 4	0.25	0	4.17	10.80	2.18
Case 5	0.25	0.25	4.17	10.82	2.24
Case 6	0.25	0.50	4.17	10.91	1.16
Case 7	0.50	0	4.07	12.95	2.18
Case 8	0.50	0.25	4.07	12.98	2.23
Case 9	0.50	0.50	4.06	13.06	1.01
Worst Case	0.50	0.50	4.06	13.11	1.00

VI. CONCLUSION

A hierarchical control strategy has been proposed to improve the captured power of a heaving wave energy converter. The hierarchical concept provided two level controllers. The higher one has succeeded in providing a sub-optimal reference signal based the sea-state and at the same time respected the physical limitations of the system in terms of buoy's elevation. This technique has shown superiority compared to the conventional method in terms of maintaining design constraints and providing satisfactory performance.

The strategy is simple and of low computational coast. It has been tested with regular and irregular sea-states, nominal system and system with different perturbation scenarios. It has shown a promising results and possibility of being deployed in the field of controlling heaving wave energy converters.

REFERENCES

[1] J. Cruz, "Ocean Wave Energy, Current Status and Future Perpectives", Springer-Verlag Berlin Heidelberg, 2008. CrossRef

[2] B. Drew, A. R. Plummer and M. N. Sahinkaya, "A review of wave energy converter technology," *Proceedings of the Institution of Mechanical Engineers, Part A: Journal of Power and Energy*, vol. 223, pp. 887-902, 2009. CrossRef

[3] R. Alcorn and D. O' Sullivan, "Electrical Design for Ocean Wave and Tidal Energy Systems", London, United Kingdom: The Institution of Engineering and Technology, 2013.

[4] A. Jaen, D. Andrade and A. Santana, "Increasing the effeciency of the passive loading strategy for wave energy conversion," *Journal of Renewable and Sustainable Energy*, vol. 5, p. 053132, 2013. CrossRef

[5] M. Jama, A. Wahyudie, A. Assi and H. Noura, "An intelligent fuzzy logic controller for maximum power capture of point absorbers," *Energies*, vol. 7, pp. 4033-4053, 2014. CrossRef

[6] M. Schoen, J. Hals and T. Moan, "Wave prediction and robust control of heaving wave energy devices for irregular waves," *IEEE Transactions on Sustainable Energy,* vol. 26, pp. 627-638, 2011. CrossRef

[7] G. Li and M. Belmont, "Model predictive control of sea wave energy converters part ii: The case of an array of devices," *Renewable Energy*, vol. 68, pp. 540-549, 2014. CrossRef

[8] M. Richter, M. Magana, O. Sawodny and T. Brekken, "Nonlinear model predictive control of a point absorber wave energy converter," *IEEE Transactions on Sustainable Energy*, vol. 4, pp. 118-126, 2013. CrossRef

[9] J. Falnes, "Ocean Waves and Oscillating Systems", Cambridge University Press, 2002. CrossRef

[10] M. Jama, H. Noura, A. Wahyudie and A. Assi, "Enhancing the performance of heaving wave energy converters using model-free control approach," *Renewable Energy*, vol. 83, pp. 931-941, 2015. CrossRef

[11] F. Fusco and J. Ringwood, "A simple and effective real-time controller for wave energy converters," *IEEE Transactions on Sustainable Energy*, vol. 4, pp. 21-30, 2014. CrossRef

[12] F. Fusco and J. Ringwood, "Hierarchical robust control of oscillating wave energy converters with uncertain dynamic," *IEEE Transactions on Sustainable Energy*, vol. 5, pp. 598-966, 2014. CrossRef

[13] T. Brekken, "On model predictive control for a point absorber wave energy 174 converter," in *IEEE Trondheim PowerTech*, Trondheim, Norway, 2011.

[14] A. Wahyudie, M. A. Jama, O. Saeed, H. Noura, A. Assi and K. Harib, "Robust and low computational cost controller for improving captured power in heaving wave energy converters," *Renewable Energy*, vol. 82, pp. 114-124, 2015. CrossRef

[15] O. Danielsson, "Wave energy conversion: Linear synchronous permanent magnet generator," Ph.D. dissertation, Uppsala University, 2006.

[16] R. Taghipoura, T. Pereza and T. Moan, "Hybrid frequency-time domain models for dynamic response analysis of marine structurres," *Ocean Engineering*, vol. 35, pp. 685-705, 2008. CrossRef

[17] W. Cummins, "The impulse response functions and ship motions," *Schiff-stechnik*, vol. 9, p. 101, 1961.

[18] G. D. Backer, "Hydrodynamic design optimization of wave energy converters consisting of heaving point absorbers," Ph.D. dissertation, University of Ghent, 2010.

[19] M. Eriksson, "Modelling and experimental verification of direct drive wave energy conversion," Ph.D. dissertation, Uppsala University, 2007.

[20] Z. Ballard and B. Mann, "Two-dimenssional nonlinear analysis of an untethered spherical buoy due to wave loading," *Journal of Computational and Nonlinear Dynamics*, vol. 8, pp. 041019(1)-041019(2), 2013.

[21] C. Canudas, H. Olsson, K. Astrom and P. Lischinsky, "A new model for control of systems with friction," *IEEE Transactions on Automatic Control*, vol. 40, pp. 419-425, 1995. CrossRef

[22] W. Xie, "Sliding-mode-observer-based adaptive control for servo actuator with friction," *IEEE Transactions on Industrial Electronics*, vol. 54, pp. 1517-1527, 2007. CrossRef

[23] M. Leijon, O. Danielsson, M. Eriksson, K. Thorburn, H. Bernhoff, J. Isberg, J. Sundberg, I. Ivanova, E. Sjostedt, O. Agren, K. Karlsson and A. Wolfbrandt, "An electrical approach to wave energy conversion," *Renewable Energy*, vol. 31, pp. 1309-1319, 2006. CrossRef

[24] J. E. Slotine and W. Li, Applied Nonlinear Control, Prentice Hall, 1991.

[25] J. Falnes, "A review of wave-energy extraction," *Renewable Energy*, vol. 20, pp. 185-201, 2007. CrossRef

[26] J. Hals, J. Falnes and T. Moan, "Constrained optimal control of a heaving buoy wave-energy converter," *Journal of Offshore Mechanics Arctic Eng.*, vol. 133, p. 011401, 2010. CrossRef

[27] X. S. Yang, Engineering Optimization: An Introduction with Metaheuristic Applications, John Wiley and Sons, 2010. CrossRef

[28] A. Santana, A. Jaen and D. Andrade, "Maximizing output power of linear generators for wave energy conversion," *International Transactions on Electrical Energy Systems*, vol. 24, p. 875890, 2014.

[29] M. Jama, "Control strategies for improving the performance of heaving wave energy converters," Ph.D. dissertation, United Arab Emirates University, 2015.

[30] K. Nielsen and T. Pontes, "Ocean energy systems' report: Annex ii task 1.1 generic and site related wave energy data," March 2010. [Online]. VIEW

[31] M. Jama, A. Wahyudie, A. Assi and H. Noura, "Controlling heaving wave energy converter using function-based model predictive control technique," *Control and Decision Conference (CCDC)*, pp. 2705-2710, 2013. CrossRef